

## Supporting Information

### High Efficient Electrochemical Conversion of CO<sub>2</sub> and NaCl to CO and NaClO

*Fengjiao Quan, Guangming Zhan, Huan Shang, Yahui Huang, Falong Jia\*, Lizhi Zhang, Zihui Ai\**

Key Laboratory of Pesticide & Chemical Biology of Ministry of Education, Institute of Applied & Environmental Chemistry, College of Chemistry, Central China Normal University, Wuhan 430079,

P. R. China

---

\* To whom correspondence should be addressed. E-mail: [fljia@mail.ccnu.edu.cn](mailto:fljia@mail.ccnu.edu.cn); [jennifer.ai@mail.ccnu.edu.cn](mailto:jennifer.ai@mail.ccnu.edu.cn)  
Phone/Fax: +86-27-6786 7535

## 1. Experimental Section

### 1.1 Reagents

Zinc nitrate hexahydrate (98%, Alfa Aesar), 2-methylimidazole (Alfa Aesar), Iron(III) 2,4-pentanedionate powder ( $\text{Fe}(\text{acac})_3$ , 99%, Alfa Aesar), methanol (Merck), Tetrahydrofuran (Sinopharm Chemical Reagent), N,N-diethyl-p-phenylenediamine (Alfa Aesar), potassium iodide (Aladdin), Nafion D-521 dispersion (5% w/w in water and 1-propanol) (Alfa Aesar). All the chemicals were of analytical grade and used without further purification.

### 1.2 Synthesis of Fe-SAs/N-C and Fe-NPs/N-C samples

The initial zeolitic imidazolate frameworks (ZIF-8) was first synthesized in methanol with reference to a typical method.<sup>1</sup> In a typical procedure, 2-methylimidazole (0.616 g) was dissolved in 15 mL of methanol with stirring in flask A.  $\text{Zn}(\text{NO}_3)_2 \cdot 6\text{H}_2\text{O}$  (0.558 g) was dissolved in 15 mL of methanol under ultrasound for 10 min to form a clear solution in flask B. Then, the solution in flask B was subsequently added into flask A under ultrasound for 10 min at room temperature. The mixed solution was transferred into a thermostatic water bath at 35 °C for 12 h. The obtained product of ZIF-8 was separated by centrifugation, washed with methanol and dried at 70 °C under vacuum.

Then, 100 mg of ZIF-8 powder was dispersed in 20 mL of tetrahydrofuran solution containing 28.2 mg of  $\text{Fe}(\text{acac})_3$ . This mixture was subjected to ultrasonic treatment (200 W) for 2 h at room temperature. After that, the tetrahydrofuran solvent was removed by vacuum and the red powder was heated at 65 °C for 6 h under vacuum. The powder was then placed in a tube furnace and heated to 950 °C at a rate of 5 °C  $\text{min}^{-1}$ , and kept at 950 °C for 3h under flowing argon gas.<sup>2</sup> After that, the furnace naturally cooled to room temperature and the obtained sample was labeled as Fe-SAs/N-C.

As for the synthesis of Fe nanoparticles loaded on carbon substrate, all the processes were same except that the amount of  $\text{Fe}(\text{acac})_3$  was adjusted to 141 mg. And the obtained sample was labeled as Fe-NPs/N-C.

As for the synthesis of sample without loading of Fe, all the processes were same except that no  $\text{Fe}(\text{acac})_3$  was added. The obtained sample was labeled as N-C.

### 1.3 Characterization

Powder X-ray diffraction patterns of samples were recorded on a Philips MPD 18801 diffraction-meter ( $\text{CuK}\alpha$  radiation,  $\lambda = 1.5418 \text{ \AA}$ , 20kV, 150mA). TEM and high resolution TEM analysis were performed by using JEM 2010 FEF TEM operating at a voltage of 200 kV. Aberration-corrected High-angle annular dark-field scanning transmission electron microscopy (HAADF-STEM) images of samples were performed with a high-resolution transmission electron microscope (JEOL JEM-2010 LaB6) operated at 200 kV. Energy dispersive spectrometer (EDS) measurement was performed by using Oxford INCA. Elemental analysis of Fe in the solid samples was detected by inductively coupled plasma atomic emission spectrometry (Optima 7300 DV). X-ray photoelectron spectroscopy (XPS) was collected on scanning X-ray microprobe (PHI 5000 Versa, ULAC-PHI, Inc.) using Al Ka radiation and the C1s peak at 284.8 eV as internal standard. Elemental mappings were collected by a Gatan GIF Quantum 965 instrument.

### 1.4 XAFS measurement and data analysis

The Fe K-edge X-ray absorption fine structure spectra were performed at the beam line 1W1B of Beijing Synchrotron Radiation Facility (BSRF), Institute of High Energy Physics (IHEP), Chinese Academy of Sciences (CAS). The storage ring was working at the energy of 2.5 GeV with a maximum current of 250 mA. The hard X-ray was monochromatized with Si(111) double-crystals. The Fe K-edge XANES data were recorded in a fluorescence mode with the references of Fe foil and  $\text{Fe}_2\text{O}_3$ . The acquired EXAFS data were extracted and processed according to the standard procedures using the ATHENA module implemented in the IFEFFIT software packages. The  $k^3$ -weighted EXAFS spectra were obtained by subtracting the post-edge background from the overall absorption and then normalizing with respect to the edge-jump step. Subsequently,  $k^3$ -weighted  $\chi(k)$  data of Fe K-edge were Fourier transformed to real (R) space using a hanning windows ( $d_k=1.0 \text{ \AA}^{-1}$ ) to separate the EXAFS contributions from different coordination shells. To obtain the quantitative structural

parameters around central atoms, least-squares curve parameter fitting was performed using the ARTEMIS module of IFEFFIT software packages.<sup>3</sup>

## 1.5 Electrochemical Measurement

All the electrochemical measurements were carried out in a conventional three-electrode system driven by CHI 660d electrochemical station (Shanghai Chenhua, China). A saturated calomel electrode (SCE) and a platinum plate were used as reference electrode and counter electrode, respectively. The working electrode was fabricated through loading of as-synthesized samples onto a glassy carbon (GC) plate (7 mm<sup>2</sup> exposed area) by the following steps. At first, 10 mg of catalysts (Fe-SAs/N-C or Fe-NPs/N-C) was dispersed in 1 mL of Nafion solution (2 wt.% in isopropanol) and then sonicated for 1h to form a homogeneous catalyst ink. Then 5  $\mu$ L of the catalyst ink was dropped onto the GC surface and dried at room temperature. Before tests, high-purified CO<sub>2</sub> (> 99.999%) gas was bubbled into the electrolyte for 30 min to achieve saturation of CO<sub>2</sub>. The linear sweep voltammetry (LSV) tests were measured in Ar- and CO<sub>2</sub>-saturated electrolyte (0.5 M NaCl solution) with three electrodes in a single cell. The potentials in the study were reported versus RHE with the conversion equation:  $E$  (vs. RHE/V) =  $E$  (vs. SCE/V) + 0.241 + 0.0591 pH.

As for the evaluation of catalysts in CO<sub>2</sub>RR process, another GC plate (2 cm<sup>2</sup> exposed area) was used as support for working electrode, and 0.2 mL of catalyst ink was coated on the GC surface (1 cm<sup>2</sup> fixed area) by the same way mentioned above. The area of the catalyst supported by the glassy carbon electrode was fixed as 1 cm<sup>2</sup> with kapton tape (Uline) in advance. After that, these three electrodes was assembled into a H-type cell which was also adopted in our previous work.<sup>4</sup> The cathode and anodic compartments were all filled with 16 mL of NaCl electrolyte and continuously purged with CO<sub>2</sub> at a flow rate of 20 mL min<sup>-1</sup>. Electrochemical reduction of CO<sub>2</sub> was conducted at various applied potentials and the gaseous products and remaining CO<sub>2</sub> were directly introduced into a gas chromatography (GC-2030, Hengxin) equipped with packed column (ZKAT-Z13 PLOT, ATEO) to realize the separation of CO<sub>2</sub> and products. And these gases would flow through a Nickel methanizer, and the CO and unreacted CO<sub>2</sub> were converted to detectable methane, which could be detected by a flame ionization detector. The following quantification was performed based on the

correlation of the concentration of gases and corresponding peak areas. The Faradaic efficiency for the product was calculated based on the average of three repeated experiments at 30 min. The Faradaic efficiency for CO is calculated by the equation (1).<sup>5</sup>

$$FE_{CO} (\%) = \frac{\text{Detected products (mol CO)} \times \frac{2 \text{ mol e}^-}{\text{mol CO}}}{\frac{\text{Electrolysis charge (C)}}{96485 \frac{\text{C}}{\text{mol e}^-}}} = \frac{\text{mol e}^- \text{ consumed by products}}{\text{mol e}^- \text{ passed through electrode}} \quad (1)$$

As for the combined electrolysis with CO<sub>2</sub>RR and anodic production of hypochlorite, a commercial ruthenium oxide (RuO<sub>2</sub>) coated titanium electrode was used as counter electrode in the anode compartment. RuO<sub>2</sub> coated titanium electrode was purchased from Chemical Corporation (Alfa aesar) and cleaned by ultrasonic treatment in acetone before use. The working area of the electrode was fixed at 2 cm<sup>2</sup> in the electrochemical experiments. The cathode compartment is the same as the compartment of CO<sub>2</sub>RR mentioned above. The electrochemical experiments were performed in 0.5 M NaCl solution at room temperature of 25 °C. The pH of the anodic electrolyte was not adjusted by additional alkaline or acid, and its value was measured to be 7.2. Constant potential was applied to working electrodes and the total consumed charge was monitored. After electrolysis with total consumed charge of 10 C, the gaseous products were analyzed by gas chromatography and the generated hypochlorite in solution was analyzed by DPD (N,N-diethyl-p-phenylenediamine) reagents with UV-vis spectrophotometry method. Firstly, 1mL of the sample solution was diluted with deionized water to 10 mL in the colorimetric cylinder (10 mL), and then 1 mL phosphate buffer (pH = 6.5) and 1 mL of DPD reagent were added into the above solution. Finally, 3 mL of above solution was transferred into 10 mm cuvette for measurement of light absorbance at 530 nm as soon as possible. During the test, the deionized water was used as the reference. The light absorbance at 530 nm can be obtained through the UV-vis 2500 spectrophotometer (Shimadzu, Japan). The calibration curve is plotted from light absorbance versus the concentration of total hypochlorite. The Faradaic efficiency for the product was calculated based on the average of three repeated experiments at 30 min. The Faradaic efficiency for ClO<sup>-</sup> is calculated by the equation (2).

$$FE_{ClO^-}(\%) = \frac{\text{Detected products (mol } ClO^-) \times \frac{2 \text{ mol } e^-}{\text{mol } ClO^-}}{\frac{\text{Electrolysis charge (C)}}{96485 \frac{C}{\text{mol } e^-}}} = \frac{\text{mol } e^- \text{ consumed by products}}{\text{mol } e^- \text{ passed through electrode}} \quad (2)$$

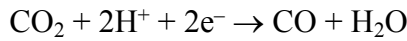
The energy efficiency of the process was calculated by the following equation (3).

$$\text{Energy efficiency} = \frac{FE_{CO}(\%) \times FE_{ClO^-}(\%) \times \text{Theoretic voltage}}{\text{Cell voltage}} \quad (3)$$

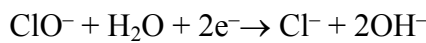
Theoretic voltage represents the difference between the half reaction potentials for the chloride oxidation and reduction  $CO_2$  to  $CO$ , which is represented by the following equation (4).

$$\text{Theoretic voltage} = E_{ClO^-/Cl^-} - E_{CO_2/CO} \quad (4)$$

Detailed calculation steps were listed in the below (assuming the activities of  $H^+$  and  $OH^-$  are approximately equal to their concentrations, and the activities of other species ( $CO$ ,  $CO_2$ ,  $Cl^-$  and  $ClO^-$ ) are approximately 1). The values of standard electrode potentials are from the Lange's Handbook of Chemistry.<sup>6</sup>



$$\begin{aligned} E_{CO_2/CO} &= E_{CO_2/CO}^\theta - \frac{RT}{2F} \ln \frac{a_{CO}}{a_{CO_2}(a_{H^+})^2} \\ &= -0.11 - \frac{8.314 \times 298.15}{2 \times 96485} \ln \frac{1}{(10^{-4.5})^2} = -0.38 \text{ (V)} \end{aligned}$$



$$\begin{aligned} E_{ClO^-/Cl^-} &= E_{ClO^-/Cl^-}^\theta - \frac{RT}{2F} \ln \frac{a_{Cl^-}(a_{OH^-})^2}{a_{ClO^-}} \\ &= 0.89 - \frac{8.314 \times 298.15}{2 \times 96485} \ln \frac{(10^{-6.8})^2}{1} = 1.29 \text{ (V)} \end{aligned}$$

Therefore,

$$E_{ClO^-/Cl^-} - E_{CO_2/CO} = 1.67 \text{ (V)}$$

## 1.6 Computational Details

All of the computations were performed by means of spin-polarized density functional theory (DFT) methods using the Vienna Ab initio Simulation Package (VASP) code.<sup>7, 8</sup> The exchange-correlation functionals described by Generalized Gradient Approximation (GGA) with the Perdew–Burke–Ernzerhof (PBE) functional,<sup>9</sup> using a plane-wave cut-off energy of 450 eV,<sup>8, 10</sup> and Fe-N<sub>4</sub> doped representative 4\*4 graphene super-cells to describe Fe-N<sub>4</sub>@C.<sup>3</sup> The Brillouin zone was sampled by 3\*3\*1 k-points by using the Monkhorst–Pack scheme. The vacuum thickness being larger than 20 Å between two graphene layers to avoid interactions between periodic images. Besides, six Fe atoms confined in 19\*20\*21Å cub to describe Fe cluster. During optimizations, the energy and force converged to 10<sup>-4</sup> eV/atom and 0.02 eV/Å. Thermal and zero-point energy (ZPE) corrections were calculated over G points.

The Gibbs free energy change ( $\Delta G$ ) of every elemental step was determined as follows:  $\Delta G = \Delta E + \Delta ZPE - T\Delta S$ , where  $\Delta E$  is the electronic energy difference directly obtained from DFT calculations,  $\Delta ZPE$  is the change in zero-point energies,  $T$  is the temperature ( $T = 298.15$  K), and  $\Delta S$  is the entropy change. The zero-point energies and entropies of the CO<sub>2</sub>RR species were computed from the vibrational frequencies, in which only the adsorbate vibrational modes were calculated explicitly, while the catalyst sheet was fixed. The entropies and vibrational frequencies of molecules in the gas phase were taken from the NIST database.

## Supporting Figures and Tables:

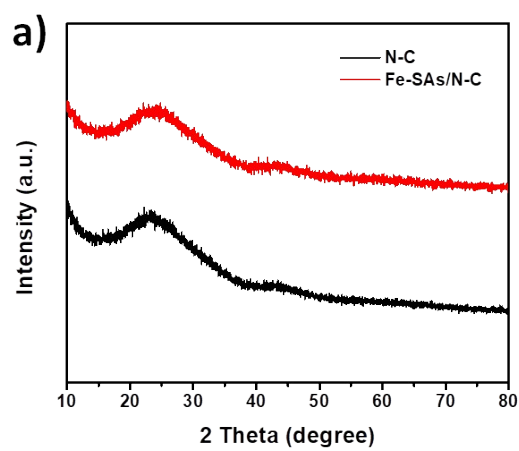


**Figure S1.** XRD patterns of the N-C and Fe-SAs/N-C samples.

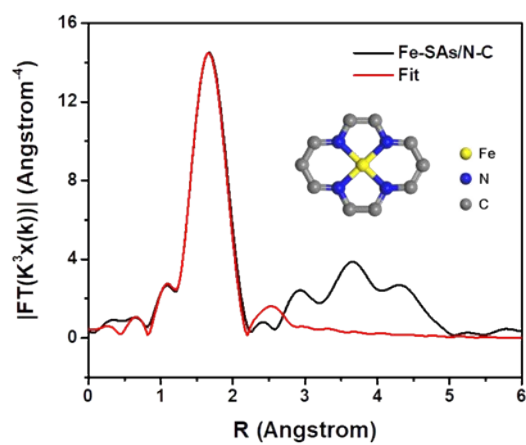


**Figure S2.** Corresponding EXAFS fitting curves for Fe-SAs/N-C sample. Inset is the schematic architecture of iron single-atom in the form of Fe-N<sub>4</sub>.

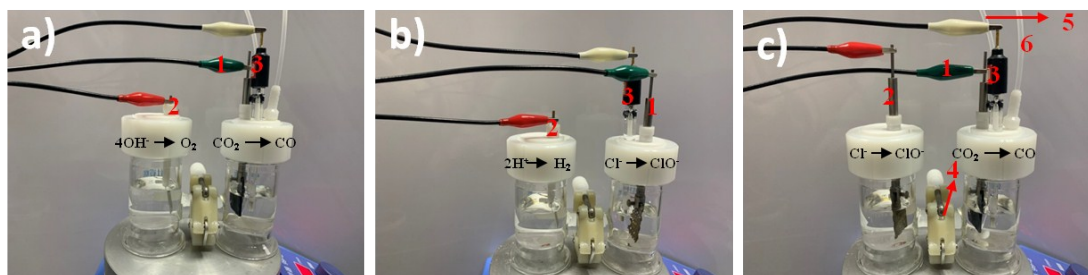


**Figure S3.** Photo images of electrochemical cells for study of CO<sub>2</sub> reduction (a), anodic oxidation of Cl<sup>-</sup> to ClO<sup>-</sup> (b) and combined electrolysis (c), respectively. The digitally marked positions in the cell are corresponded to the following components: 1. working electrode; 2. counter electrode; 3. reference electrode (saturated calomel electrode); 4. proton exchange membrane (Nafion 117); 5. gas inlet; 6. gas outlet. In cell (a), Fe-SAs/N-C (or Fe-NPs/N-C) was used as working electrode and platinum plate was used as counter electrode. In cell (b), ruthenium–titanium dioxide mesh electrode was used as working electrode and platinum plate was used as counter electrode. In cell (c), Fe-SAs/N-C was used as working electrode and ruthenium–titanium dioxide mesh electrode was used as counter electrode.

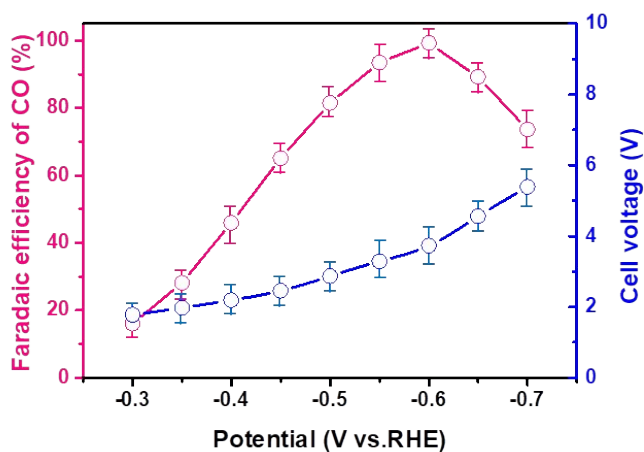


**Figure S4.** Faradaic efficiencies of CO and corresponding cell voltages versus potentials (-0.3 ~ -0.7 V) in NaHCO<sub>3</sub> solution.

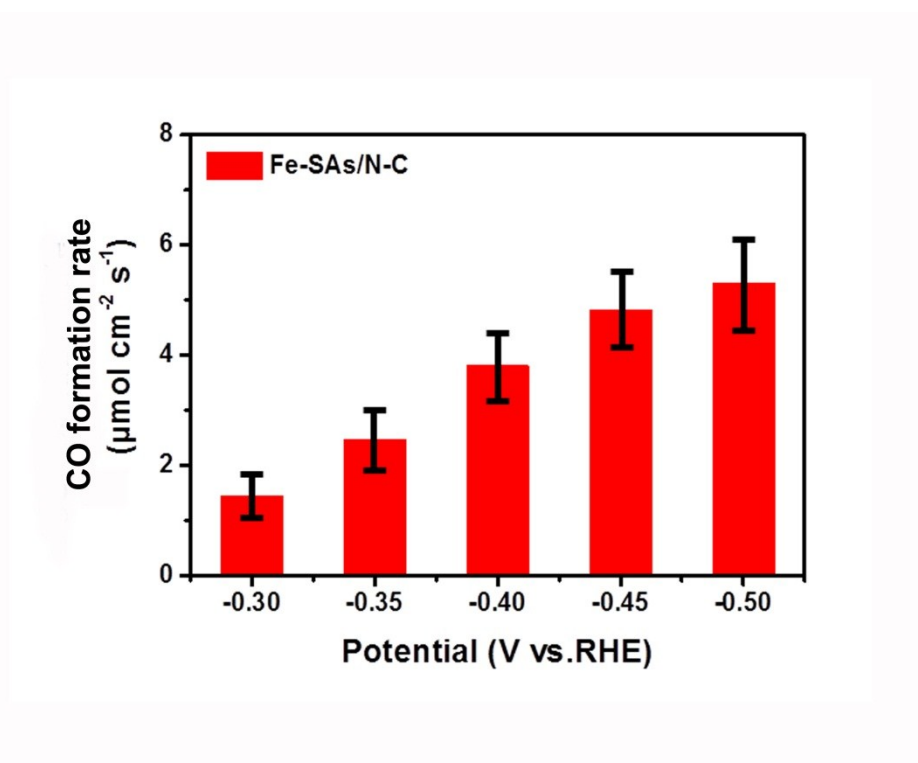


**Figure S5.** The formation rates of CO at constant potentials over Fe-SAs/N-C catalyst. The error bars are also presented in the figure.

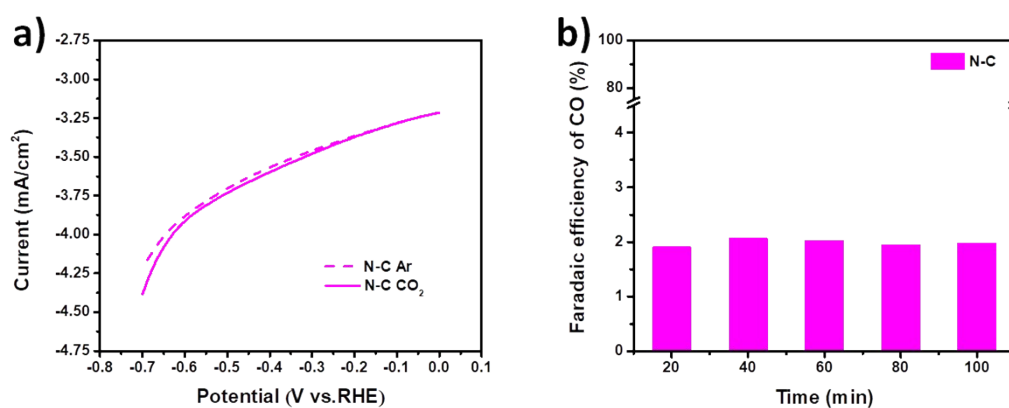


**Figure S6.** (a) LSV curves for N-C sample in the Ar-saturated (magenta dotted line) or CO<sub>2</sub>-saturated (magenta solid line) 0.5 M NaCl electrolyte at a scan rate of 50 mV s<sup>-1</sup>. (b) Faradaic efficiency of CO versus continuous electrolysis time at -0.45 V on N-C sample.

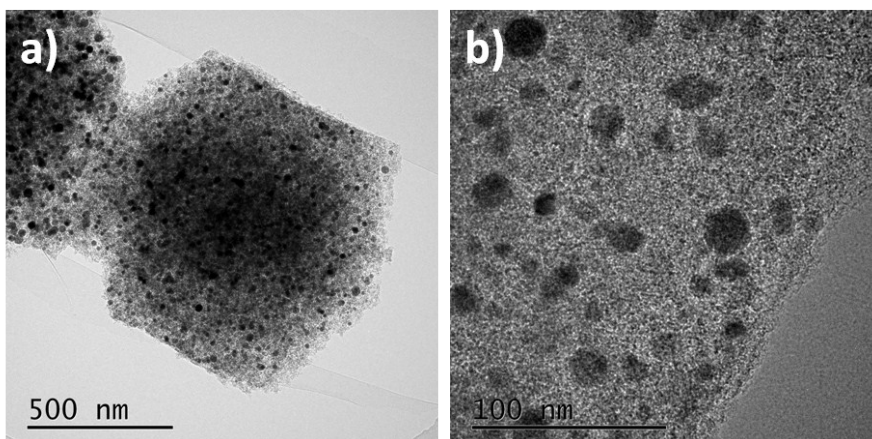


**Figure S7.** TEM images (a, b) of Fe-NPs/N-C sample.

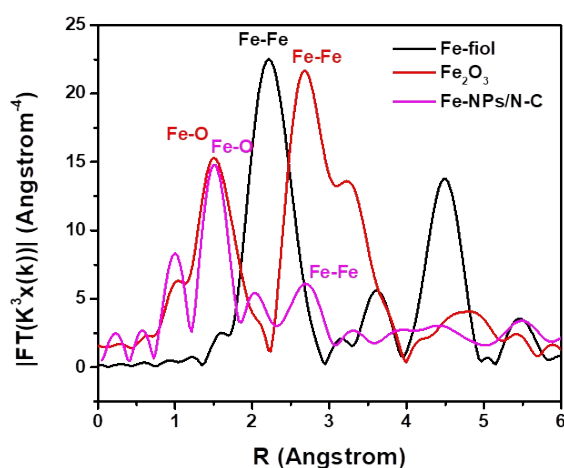


**Figure S8.** Fourier transform (FT) of the Fe K-edge of Fe NPs/N-C sample, Fe<sub>2</sub>O<sub>3</sub> and Fe foil.

The FT  $k^3$ -weighted  $\chi(k)$  function of the EXAFS spectra for Fe-NPs/N-C sample shows the main peak is closer to 1.5 Å, belonging to the Fe-O coordination. In addition, another peak at  $\sim 2.20$  Å indicates the possible presence of Fe-Fe bonding from small Fe clusters. The EXAFS result excludes the possible existence of iron single-atoms.

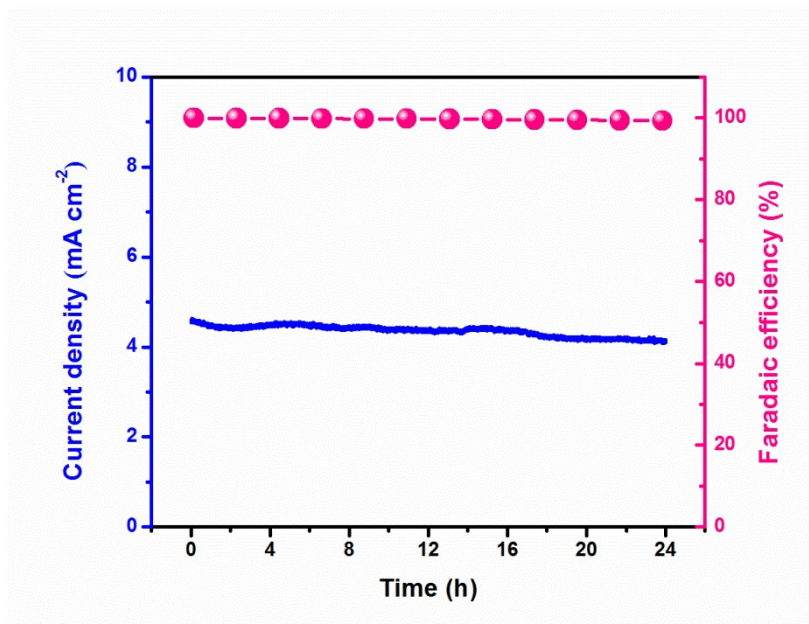


**Figure S9.** Total current density (left axis) and Faradaic efficiency of CO (right axis) versus time on Fe-SAs/N-C.

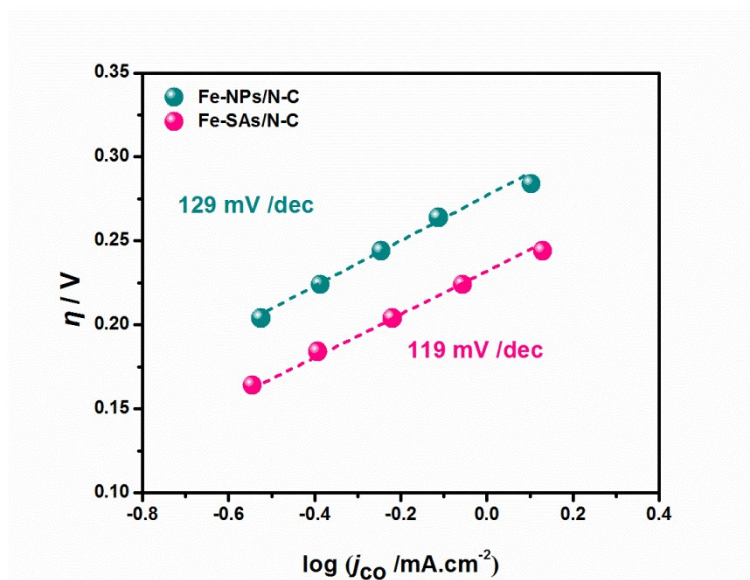


**Figure S10.** Tafel plots of overpotential against CO partial current densities achieved on Fe-SAs/N-C and Fe-NPs/N-C catalyst.

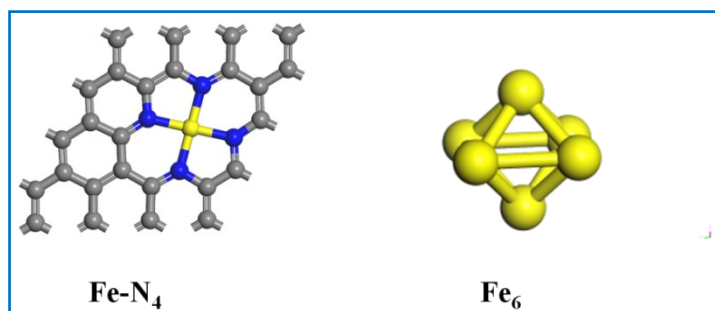


**Figure S11.** Computational models of Fe single-atom (in the form of Fe-N<sub>4</sub>) and Fe particle (in the form of Fe<sub>6</sub>).

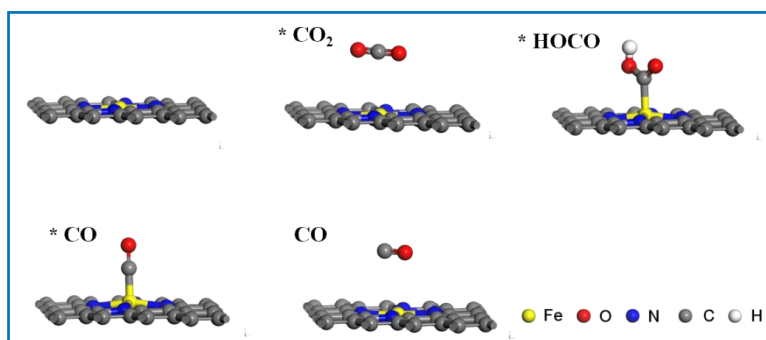


**Figure S12.** Spatial configurations of CO<sub>2</sub> and intermediates on the Fe single-atom model.

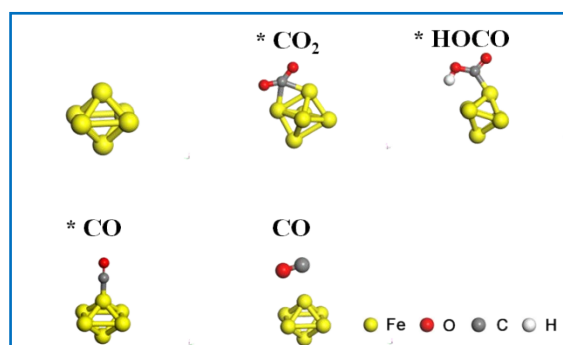


**Figure S13.** Spatial configurations of CO<sub>2</sub> and intermediates on the Fe particle model.

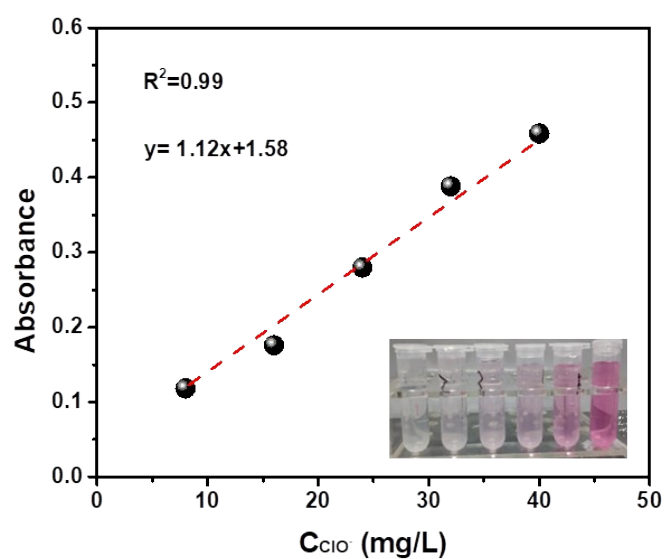


**Figure S14.** The standard curve of hypochlorite analysis.

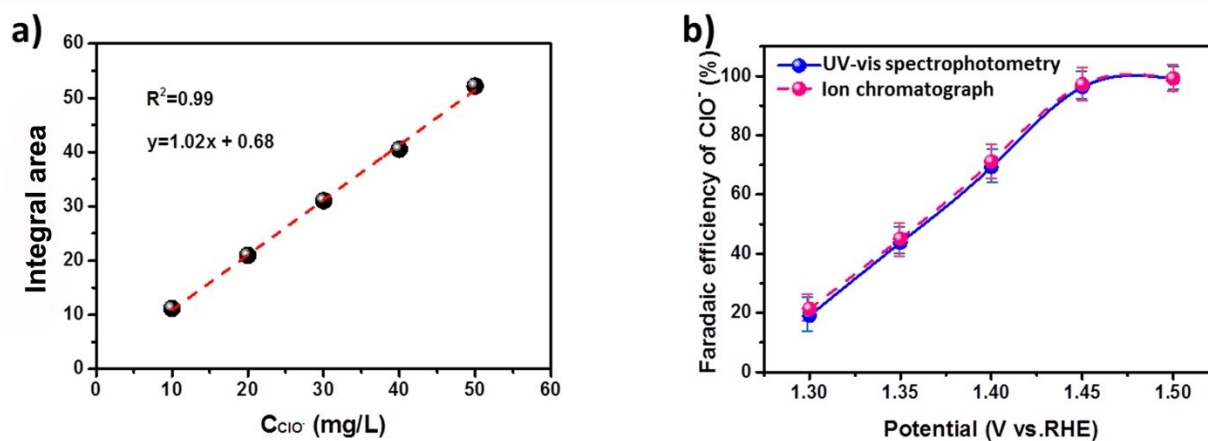


**Figure S15.** (a) Standard curve of hypochlorite measured by the ion chromatograph method. (b) Comparison of UV-vis spectrophotometry and ion chromatograph in case of determination of Faradaic efficiency of hypochlorite.

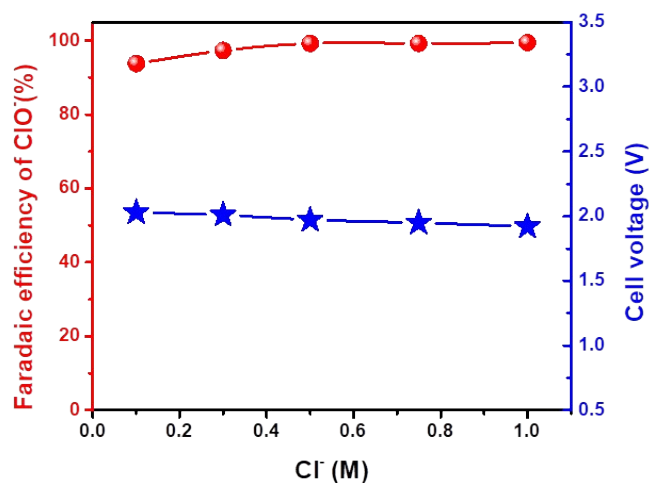


**Figure S16.** Faradaic efficiency for hypochlorite and corresponding cell voltage versus concentration of chloride at 1.1 V. The total concentration of Na<sup>+</sup> was maintained at 1.0 M by adding NaClO<sub>4</sub>.

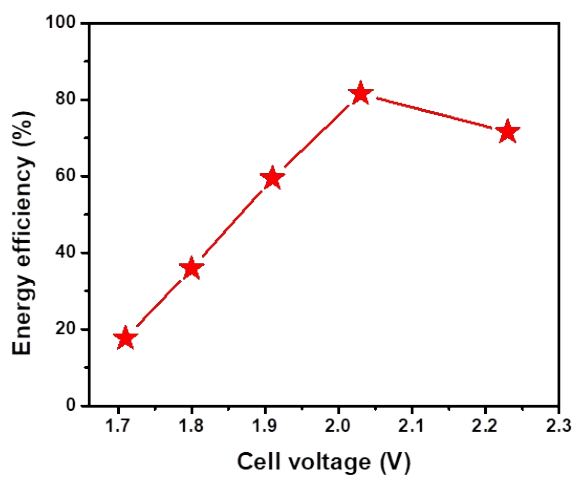


**Figure S17.** The relationship between the energy efficiency and corresponding cell voltage.

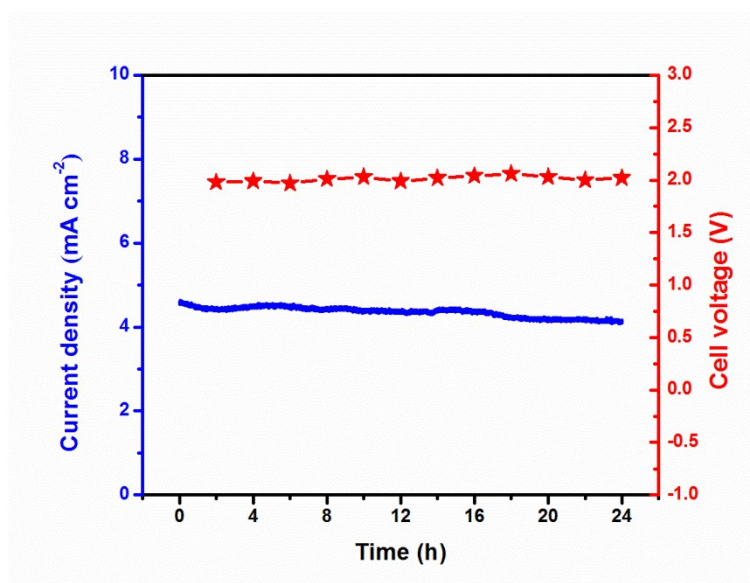


**Figure S18.** Total current density versus time on (left axis) and cell voltage versus time (right axis).

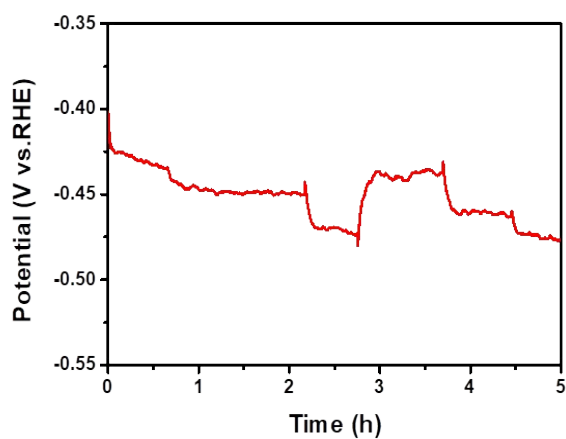


**Figure S19.** Change of cathode potential versus reaction time in the solar cell-driven electrolysis process. The cathode potential was recorded through measuring the potential difference between the cathode and a reference electrode in solar cell-driven electrolysis.

**Table S1.** Fe K-edge EXAFS curves Fitting Parameters (N, coordination number; R, distance between absorber and backscatter atoms;  $\sigma^2$ , Debye–Waller factor to account for both thermal and structural disorders;  $\Delta E^0$ , inner potential correction to account for the difference in the inner potential between the sample and the reference compound; R factor (%) indicates the goodness of the fit.)

Sample	Path	N	R(Å)	$\sigma^2 (\times 10^{-3} \text{ \AA}^2)$	$\Delta E_0$ (eV)	R, %
Fe-SAs/N-C	Fe-N(O)	3.8	1.99	4.2	-1.6	0.02

**Table S2.** Reaction energetics for the 2-electron transfer processes during CO<sub>2</sub>RR.  $\Delta E$ , energy (i.e enthalpy) change;  $\Delta G$ , free energy change at T=298 K and U= 0 V.

Elementary reactions	Fe-N <sub>4</sub>		Fe <sub>6</sub>	
	$\Delta E$	$\Delta G$	$\Delta E$	$\Delta G$
CO <sub>2</sub> + * → *CO <sub>2</sub>	0.55	-0.11	-0.13	-0.79
*CO <sub>2</sub> + H <sup>+</sup> + e <sup>-</sup> → *HOCO	0.67	0.72	1.34	1.39
*HOCO + H <sup>+</sup> + e <sup>-</sup> → *CO + H <sub>2</sub> O	-0.50	-0.35	-0.97	-0.83
*CO → CO + *	-0.15	0.46	0.38	0.95

## References

1. C. Zhao, X. Dai, T. Yao, W. Chen, X. Wang, J. Wang, J. Yang, S. Wei, Y. Wu and Y. Li, *J. Am. Chem. Soc.*, 2017, **139**, 8078-8081.
2. P. Yin, T. Yao, Y. Wu, L. Zheng, Y. Lin, W. Liu, H. Ju, J. Zhu, X. Hong, Z. Deng, G. Zhou, S. Wei and Y. Li, *Angew. Chem. Int. Edit.*, 2016, **55**, 10800-10805.
3. Y. Chen, S. Ji, Y. Wang, J. Dong, W. Chen, Z. Li, R. Shen, L. Zheng, Z. Zhuang, D. Wang and Y. Li, *Angew. Chem. Int. Edit.*, 2017, **56**, 6937-6941.
4. F. Quan, D. Zhong, H. Song, F. Jia and L. Zhang, *J. Mater. Chem. A*, 2015, **3**, 16409-16413.
5. D. R. Kauffman, J. Thakkar, R. Siva, C. Matranga, P. R. Ohodnicki, C. Zeng and R. Jin, *ACS Appl. Mater. Inter.*, 2015, **7**, 15626-15632.
6. G. S. Dr. James, in *Lange's Handbook of Chemistry, Seventeenth Edition*, McGraw Hill Professional, Access Engineering, 2017.
7. J. P. Perdew, K. Burke and M. Ernzerhof, *Phys. Rev. Lett.*, 1996, **77**, 3865-3868.
8. G. Kresse and D. Joubert, *Phys. Rev. B*, 1999, **59**, 1758-1775.
9. G. Kresse and J. Furthmüller, *Phys. Rev. B*, 1996, **54**, 11169-11186.
10. P. E. Blöchl, *Phys. Rev. B*, 1994, **50**, 17953-17979.